Development of Metal−SiO₂ Nanocomposites in a Single-Step Process by the Polymerizable Complex Method

E. R. Leite,* N. L. V. Carreño, E. Longo, and F. M. Pontes

CMDMC-LIEC, Departamento de Química, UFSCar, Via Washington Luiz, Km 235, C.P. 676 CEP 13565-905, São Carlos, SP, Brazil

A. Barison and A. G. Ferreira

Departmento de Química, UFSCar, Via Washington Luiz, São Carlos, SP, Brazil

Y. Maniette and J. A. Varela

Instituto de Química, UNESP, C.P. 355 CEP 14801-970, Araraquara, SP, Brazil

This work presents the synthesis and characterization of SiO₂:metal (Ni, Co, Ag, and Fe) nanocomposites processed by the polymerizable complex method. The polymeric precursor solutions obtained were characterized by means of FT-Raman and ^{13}C NMR spectroscopy. The results show the formation of a hybrid polymer with carbon and silicon in the macromolecule chain and the transition metal cation arrested within this polymeric chain. The nanocomposites are formed during the controlled polymeric precursor pyrolysis. The reduction of the metal cation is promoted by the CO/CO_2 atmosphere resulting from the pyrolysis of the organic material. Microstructural characterization, performed by TEM and X-ray diffraction (XRD), showed that the nanocomposites are formed by metal nanoparticles embedded in a amorphous matrix formed by SiO_2 and carbon. In the SiO_2:Fe system, Fe_3C was also detected by XRD.

1. Introduction

Transition metal nanoparticles have been extensively studied and several methods have been used to synthesize them. Because of the very high surface area-to-volume ratio, these particles have a high reactivity and can be easily environmentally degraded, forming for instance a surface oxide layer surrounding the metal particles. Another problem related to the nanometric size particles is the tendency to agglomerate. To avoid the particle agglomeration, several approaches have been adopted.[1−3] Ding and Gin[4] recently stabilized Pd nanoparticles using a cross-linked lyotropic liquid crystal, reporting good stability and good catalytic activity. With the advent of the mesoporous molecular sieves,[5,6] new possibilities to stabilize metal nanoparticles have arisen. In our point of view, the best way to solve the nanoparticle agglomeration and eventually its surface oxidation is the development of nanocomposites in which the metals are embedded in an inorganic phase. The nanocomposites approach has been used in the development of several functional materials.[7,8]

Recently,[9] we described a new route to synthesize nanometric Ni particles embedded in a mesoporous silica material with excellent potential for catalytic applications. Mesoporous silica with surface area in the range of 202−280 m²/g, with narrow pore size distribution and Ni nanoparticles (particles in the range of 3−41 nm), were obtained in a direct process, that is, in a single heat-treatment process. A different approach was adopted to process such a nanocomposite. This new approach is based on the formation of a hybrid polymer with the silicon as a component of the macromolecule chain and nickel cations arrested within the macromolecule structure and also on the control of the pyrolysis step. The CO/CO_2 atmosphere resulting from the pyrolysis of the organic material promotes the reduction of the Ni salt. The general idea of this method is to produce an amorphous SiO_2 matrix with metal nanoparticles well dispersed and embedded within this matrix (see Scheme 1) in a direct (single-step) process without a hydrogen atmosphere during the heat treatment. In fact, this process is similar to the polymeric

* To whom correspondence should be addressed. E-mail: derl@power.ufscar.br.
(1) Lin, Y.; Finke, R. G. *J. Am. Chem. Soc.* **1994,** *116,* 8335.
(2) Mecking, S.; Thomann, R. *Adv. Mater.* **2000,** *13,* 953.
(3) Zhao, M.; Crooks, R. M. *Angew. Chem. Int. Ed.* **1999,** *38,* 364.
(4) Ding, J. H.; Gin, D. L. *Chem. Mater.* **2000,** *12,* 22.
(5) Kresge, C. T.; Leonowicz, M. E.; Roth, W. J.; Vartuli, J. C.; Beck, J. S. *Nature* **1992,** *359,* 710.
(6) Brinker, C. J.; Lu, Y.; Sellinger, A.; Fan, H. *Adv. Mater.* **1999,** *11,* 579.

(7) Morris, C. A.; Anderson, M. L.; Stroud, R. M.; Merzbacher, C. I.; Rolison, D. R. *Science* **1999,** *284,* 622.
(8) (a) Sanchez, C.; de A. A. Soler-Illia, G. J.; Ribot, F.; Lalot, T.; Mayer, C. R.; Cabuil, V. *Chem. Mater.* **2001,** *13,* 3061. (b) Caruso, R. A.; Antonietti, M. *Chem. Mater.* **2001,** *13,* 3272.
(9) Leite, E. R.; Carreño, N. L. V.; Longo, E.; Valentini, A.; Probst, L. F. D. *J. Nanoscience Nanotechnology* **2002,** *2,* 89.

Scheme 1. Schematic Representation of the Target Material (Well-Dispersed Ni Nanoparticles in a Mesoporous Silica Support)
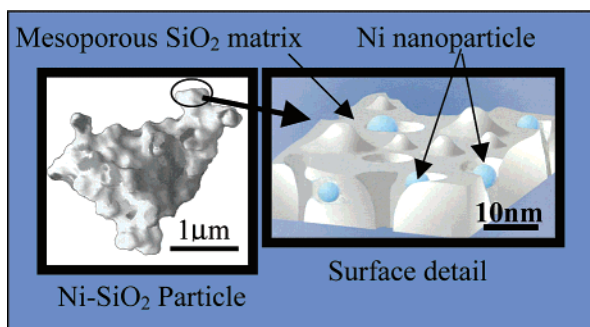
precursor method or polymerizable complex method, largely employed to process nanoparticle oxides and thin films.[10]

In this work, a more in depth analysis of the process developed by Leite et al.[9] and the application of that method to synthesize several SiO_2:metal (Ni, Co, Ag, and Fe) nanocomposites is presented.

2. Experimental Section

2.1. Synthesis. Metal nanoparticles dispersed within the mesoporous silica were synthesized by using tetraethyl orthosilicate (TEOS purity 99%, Aldrich), citric acid (CA) (purity > 99.9%, E. Merck), and the metal nitrate. CA (0.20 mol) was dissolved in 250 mL of ethanol and later the TEOS and the metal nitrate were added to the CA−ethanol solution and mixed for homogenization for 15 min, at room temperature. A citric acid/metal ratio of 3:1 (in mol) was used. The metal concentration is the sum of Si and the transition metal. The transition metals/Si ratio ranges from 4.0 to 0.25, considering all systems studied. This was confirmed later by atomic absorption measurements. Ethylene glycol (EG) was added to the citrate solutions, at a mass ratio of 40:60 in relation to the citric acid, to promote the polymerizing reaction. After polymerization at temperatures ranging from 90 to 120 °C for 3 h, the solid resin was treated at 250 °C for 3 h, in an air atmosphere. The resulting precursor compound was ground in a ball mill using zirconia balls of about 2.0-mm diameter. Later, the samples were pyrolyzed for different times at different temperatures in a N_2 atmosphere (flow rate of 1 cm³/min). Figure 1 shows a general flowchart for obtaining SiO_2−metal nanocomposites.

2.2. Spectroscopy Characterization. Liquid-state NMR spectra of ¹³C were carried out in a standard NMR spectrometer (BRUKER, DRX400 model, Germany), operating at the ¹³C resonance frequency. The chemical shift was set using TMS (tetramethylsilane) as the reference. Raman data were taken on a RFS/100 Bruker FT-Raman with a Nd:YVO₄ laser, providing an exciting wavelength at 1064 nm. The spectral resolution was 4 cm⁻¹. All the measurements were taken at room temperature.

2.3. Phase Evolution and Microstructure Characterization. The crystal structure of the transition metals was characterized by XRD (Model D-5000, Siemens, Karlsruhe, Germany), using Cu Kα radiation and a graphite monochromator. For the HRTEM/TEM (200 kV Model CM200 Philips, Holland) study, a drop of the powder suspension was deposited on a carbon-covered nickel grid. The nanocomposite powders were characterized by elementary chemical analysis to deter-
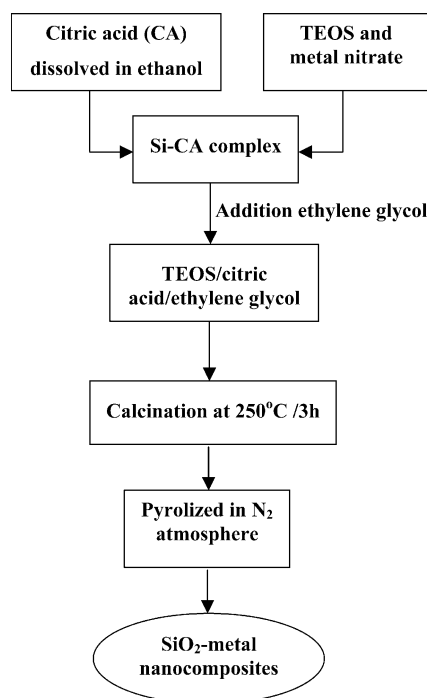
(10) For thin films references see: (a) Bouquet, V.; Leite, E. R.; Longo, E.; Varela, J. A. *J. Eur. Ceram. Soc.* **1999**, *19*, 1447. (b) Zanetti, S. M.; Leite, E. R.; Longo, E.; Varela, J. A. *J. Mater. Res.* **1998**, *13*, 2932. (c) Zanetti, S. M. Leite, E. R.; Longo, E.; Varela, J. A. *Appl. Organomet. Chem.* **1999**, *13*, 373; (d) Leite, E. R.; I. Weber, T.; Longo, E.; Varela, J. A. *Adv. Mater.* **2000**, *12*, *13*, 965.
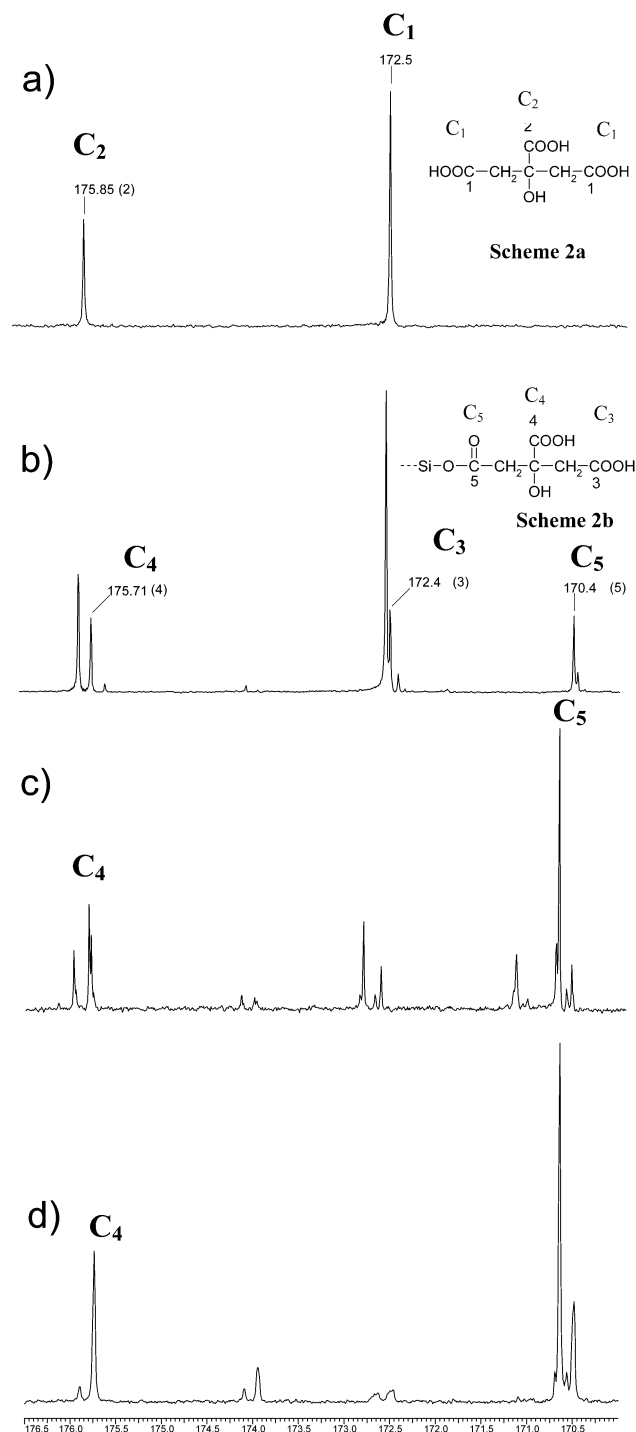

Figure 1. Synthesis flowchart of SiO_2:metal nanocomposites.

mine the total carbon content after the pyrolysis step (CHN analysis-FISONS EA 1108 CHNS-O). The pyrolysis step was followed by thermogravimetric analysis (TG) (model STA 409 Netzsch, Selb, Germany), using a 10 °C/min heating rate with a nitrogen flow of 20 cm³/min.

3. Results and Discussion

3.1. Citrate and Polymer Characterization. The process used to prepare the nanocomposites reported in this work is based on the formation of Si−citric acid (CA) complex and later polymerization of this complex through a polyesterification reaction with ethylene glycol. However, this process was not well characterized yet. To investigate the silicon complexation reaction, liquid-state ¹³C NMR was applied. Figure 2 shows the ¹³C NMR spectra of the citric acid in ethanol (Figure 2a) and TEOS plus citric acid solution just after the mixing (Figure 2b), after 168 h (Figure 2c), and after 720 h from preparation (Figure 2d), in a region of the NMR spectra related to carboxyl groups (170−190 ppm). All measurements were taken at room temperature and the molar ratio between CA and TEOS was 2:1. For convenience, the insets of parts a and b of Figure 2 show the assignment of the NMR peaks to certain carbon centers.

In the spectrum of the pure CA solution, the peaks at 172.52 and 175.85 ppm are associated with the terminal carbon (C_1) of the carboxyl group and with the carbon of the central carboxyl group (C_2), respectively. Figure 2b shows the liquid-state ¹³C NMR spectra of the TEOS/citric acid system just after mixing. In this spectrum, we can observe new features, with a peak at 170.48 ppm (C_5), besides the peak at 175.71 ppm (C_4), related to the C_2 peak, and the peak at 172.42 ppm (C_3)-related to C_1. The C_5 peak is a strong indicator that the Si complexation process (the formation of the Si−O−C bond) occurs preferentially with the terminal carboxyl group of the CA. A similar complexation process was

a)

C$_1$
172.5

C$_2$
175.85 (2)

C$_2$
∠
COOH
C$_1$ C$_1$
HOOC—CH$_2$—C—CH$_2$—COOH
1   OH   1

Scheme 2a

b)

C$_4$
4
COOH
C$_5$ C$_3$
O
⋯Si—O—C—CH$_2$—C—CH$_2$—COOH
5   OH   3

Scheme 2b

C$_4$
175.71 (4)

C$_3$
172.4 (3)

C$_5$
170.4 (5)

C$_5$

c)

C$_5$

C$_4$

d) C$_4$

176.5 176.0 175.5 175.0 174.5 174.0 173.5 173.0 172.5 172.0 171.5 171.0 170.5

Figure 2. ^{13}C NMR spectra of the system investigated with (a) citric acid, (b) citric acid /TEOS, (c) citric acid/TEOS after 168 h of reaction, and (d) citric acid/TEOS after 720 h of reaction.

reported by Kakihana et al.[11,12] for the Ti—Ba—citric acid complex. This result confirms the formation of the Si—CA complex. The chemical shift between C$_3$ and C$_1$ peaks and between C$_4$ and C$_2$ peaks must be related to the new chemical environment promoted by the Si complexation. The spectra of parts c and d of Figure 2

(11) Kakihana, M.; Yoshimura, M. *Bull. Chem. Soc. Jpn.* **1999**, *72*, 1427.
(12) Kakihana, M.; Arima, M.; Nakamura, Y.; Yashima, M.; Yoshimura, M. *Chem. Mater.* **1999**, *11*, 438.

Intensity (Arbitrary Units)

(e)

(d)

(c)

2 1

(b)

(a)

2000   1500
Wavenumber (cm^{-1})

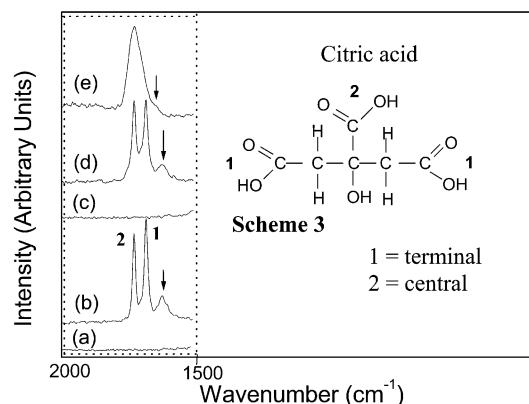Citric acid

Scheme 3

1 = terminal
2 = central

Figure 3. FT-Raman spectra of the system investigated with (a) ethylene glycol, (b) citric acid, (c) TEOS, (d) TEOS/citric acid, and (e) TEOS/citric acid/ethylene glycol.

show that the Si complexation process follows the same tendency, with a preferential reaction of the Si with the terminal carboxyl group. After 720 h, practically all terminal carboxyl groups of the CA have already reacted with the Si, resulting in the Si—CA complex. These results suggest the following reaction between the TEOS and CA, in ethanol:

$$Si(OC_2H_5)_4 + 2COH(COOH)[CH_2(COOH)]_2 \rightarrow$$
$$Si\{[COH(COOH)][CH_2(COO)]_2\}_2 + 4C_2H_5OH \quad (1)$$
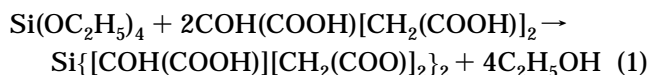
The ^{13}C NMR analysis indicates also that the central carboxyl group basically is not used during the Si—CA complex formation. This suggests that the central carboxyl group can be used in a later polymerization reaction.

The previous experiments were done at room temperature. At the reaction conditions used during the polymeric precursor preparation, temperatures in the range of 90—120 °C, the Si—CA complex formation must be accelerated, resulting in a complete complexation reaction in a few minutes.

The Si—CA complex and the polymerization process were also followed by FT-Raman spectroscopy. Figure 3 shows the FT-Raman spectra of ethylene glycol (a), citric acid (CA) (b), TEOS (c), TEOS + citric acid (1:2 molar ratio) reacted at 80 °C for several hours (d), and TEOS + citric acid + ethylene glycol (1:2:4 molar ratio) reacted at 80 °C for several hours (e). Both the Si—citric acid complex formation and polymerization must involve the carboxyl groups of the CA. Thus, all our analyses in the FT-Raman experiments will be concentrated in the spectral range related to this organic group (1800—1600-cm^{-1} wavenumber range).

The spectrum of citric acid (CA) (Figure 3b) presents two intense peaks at 1736 and 1692 and one weak and broad peak at 1634 cm^{-1}, which are assigned to the carboxyl groups (—COOH).[13] The two strong and sharp peaks (1736 and 1692 cm^{-1}) can be assigned to the stretching of the central carboxyl ν(C=O) and to the stretching of the terminal carboxyl ν(C=O), respectively. The weak and broad peak at 1634 cm^{-1} is attributable to the stretching vibration of the carboxyl group related to a strong intramolecular hydrogen bond.[13] Thus, this

(13) Tarakeshwar, P.; Manogran, S. *Spectrochim. Acta* **1994**, *50A*, 2327.

weak peak is not suitable for following the reaction between the Si and the carboxyl groups but can be used for identifying modifications in the intramolecular hydrogen bond after the complex formation. Modification in the central and terminal peaks (see Scheme 3 in Figure 3) can indicate the formation of the Si−CA complex and polymeric gel. It is important to point out that the ethylene glycol and TEOS did not present characteristic bands in this spectral range.

After the reaction between CA and TEOS we observed modifications in the peaks at 1692 and 1634 cm^{-1} (Figure 3d). We noticed that the peak at 1692 cm^{-1} became less intense in relation to the peak at 1732 cm^{-1} and that the peak at 1634 cm^{-1} became broader. The decrease in the intensity of the terminal carboxyl ν(C= O) stretching peak is an indicator of the bond formation between Si and O. No significant Raman shift of the central and terminal −COOH groups, in relation to CA, was observed after the reaction between TEOS and CA. This result suggests that the C−O−Si bond formation did not promote the weakening of bond strength between C and O atoms of the C=O group. Other indicators of the Si−CA complex formation is the modification in the peak related to the interaction between carboxyl groups. The modification in the intramolecular hydrogen bond after the Si−CA complex formation is natural.

We will now discuss the results obtained by the FT-Raman analysis of the TEOS + citric acid + ethylene glycol (EG) sample (Figure 3e). We can notice that the three peaks associated with the carboxyl ν(C=O) stretching peak in the CA and Si−CA complex were transformed in a broad and single peak centered at 1732 cm^{-1} and in a shoulder above 1660 cm^{-1}. These results confirm the reaction between the Si−CA complex and the EG. The broad and single shifted peak observed after the polymerization reaction must be an indicator of a branch polymer formation. The shoulder centered at 1660 cm^{-1} can be associated with an intramolecular hydrogen bond between the carboxyl groups. The Raman shift (in relation to the CA and Si−CA complex) observed for this peak suggests a modification in the intramolecular strength after the polymerization reaction.

The study of ^{13}C NMR and Raman spectroscopy clearly showed the reaction between the CA and TEOS, at room temperature, resulting in a Si−CA complex. FT-Raman analysis confirmed the polymerization reaction of the Si−CA complex with EG. These results indicate the formation of an organic−inorganic (hybrid) polymer. With the addition of metallic nitrates, the metallic cations are arrested within the organic−inorganic macromolecules, promoting the distribution of the cation at a molecular level. In this stage of the process, we have a polymeric precursor with Si in the chain of the hybrid polymer and the metallic cations arrested within this polymer. We believe that the distribution of the metallic cation at molecular level must provide a very good distribution of the metallic particles in the silica matrix after the pyrolysis of the polymeric precursor.

3.2. Nanocomposite Phase Formation Study. The nanocomposite will be formed through the pyrolysis of the polymeric precursor. This pyrolysis is done in two steps. The first one promotes the breakage of the organic part of the polymeric precursor. In this step, the
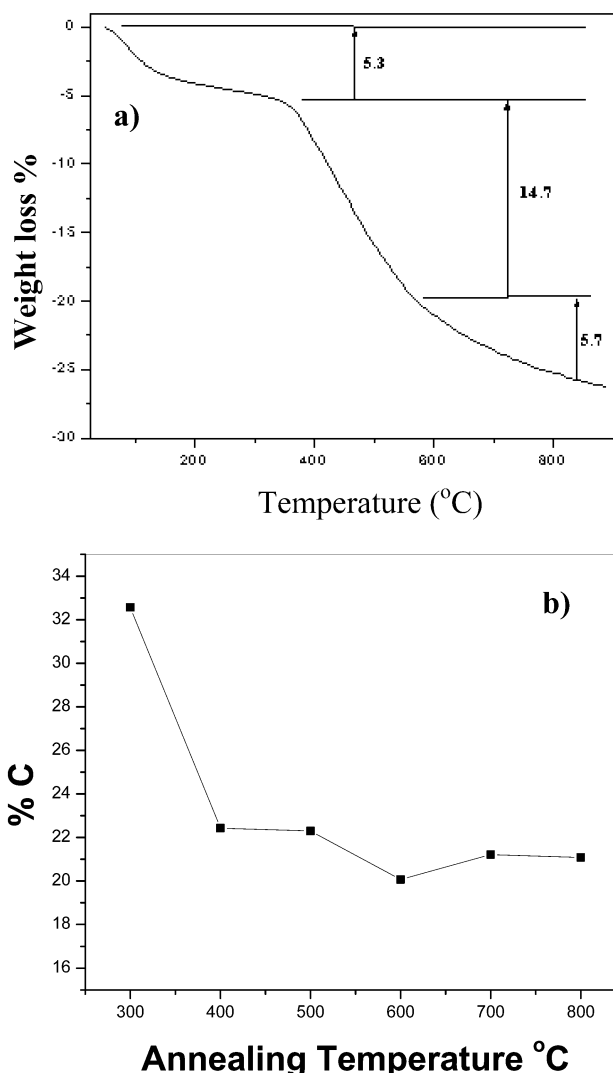

Figure 4. (a) Thermogravimetric analysis of the SiO₂:Ni (≈23.0 wt % Ni) nanocomposite. In this experiment a heating rate of 10 °C/min, 10 mg of sample, and nitrogen flow of 50 cm³/min were used. (b) The elementary chemical analysis (% C) as a function of the heat-treatment temperature of the SiO₂: Ni (≈23.0 wt % Ni) nanocomposites.

polymeric precursor is heat-treated at 250 °C for 3 h, in air. This temperature was chosen based on the thermogravimetric analysis. Figure 4a shows a typical thermogravimetric analysis of the polymeric precursor, for the SiO₂:Ni (≈23.0 wt %Ni) sample. We can observe a well-defined weight loss at around 200 °C, which was associated with the breakage of the organic part of the hybrid polymeric precursor. After this step, the material is milled in a ball mill, resulting in a fine powder.

This fine powder is submitted to a second pyrolysis treatment (the second step), but now in a N₂ atmosphere, at temperatures higher than 400 °C. Once again this temperature was chosen based on the thermogravimetric analysis (see Figure 4a). We can observe that the highest weight loss occurs between 400 and 500 °C. It is in this second stage that the nanocomposite will be formed. As we can see in Figure 4a, the weight loss rate decreases for temperatures higher than 500 °C. Figure 4b presents the carbon content (determined by CHN measurements) as a function of the heat-treatment temperature, during the second pyrolysis step, for the

Table 1. Crystallite Size (X-ray Average Diameter) of the Transition-Metal Particles for Different SiO₂:Metal Ratios and Different Pyrolysis Temperatures

samples	pyrolysis temperature (°C)	crystallite size (nm)
SiO₂:Co (≈45.0 wt % Co)	775, 1 h	81.1
SiO₂:Co (≈15.0 wt % Co)	700, 1 h	26.2
SiO₂:Ni (≈5 wt % Ni)	500, 2 h	4.8
SiO₂:Ni (≈12.5 wt % Ni)	500, 2 h	5.4
SiO₂:Ni (≈23.0 wt % Ni)	500, 2 h	3.4
SiO₂:Ni (≈46.0 wt % Ni)	500, 2 h	3.8
SiO₂:Ag (≈1.0 wt % Ag)	350, 2 h	13.6
SiO₂: Ag (~1.0 wt %Ag)	500, 2h	45.3

SiO₂:Ni (≈23.0 wt %Ni) sample. The CHN analyses reveal that after the second heat-treatment step a carbon phase is formed, besides the metallic and the silica phases. The total weight loss obtained by the TG measurements and the carbon concentration obtained by CHN changed for the different SiO₂:metal systems studied and also for different metal concentrations. However, always the formation of a carbon phase was observed.

The X-ray diffraction (XRD) patterns presented in Figure 5, considering several nanocomposites systems,

confirm the reduction of the Ni, Co, Ag, and Fe salts and the formation of metal particles. These XRD patterns show also that the silica and carbon phase formed during the second step are in the amorphous state. The crystallite size of the metallic component of the nanocomposite (Ni, Co, Ag, and Fe) was determined based on the diffraction peak (111) of (Ni, Co, Ag) and (110) of Fe, respectively, and the Scherrer equation.[14] In this study, the diffraction peak profile was fitted using a pseudo-Voigt function to calculate the full-width at half-maximum (fwhm). The obtained values are listed in Table 1 and we can observe that the metallic phase presents nanometric dimensions (particles <100 nm).

The XRD patterns of the SiO₂:Co (containing 45 wt % of Co) nanocomposites, displayed in parts a−c of Figure 5, show that the increase of the annealing temperature promotes a gradual transition from hexagonal (hcp) Co to cubic (fcc) Co. At the highest heat-treatment temperature used (775 °C), only cubic Co is observed, while at the lowest temperature (500 °C) we can observe the phase coexistence between hcp and fcc Co.

Considering the SiO₂:Fe system (Figure 5d), besides the metallic iron phase, iron carbide (Fe₃C) was also
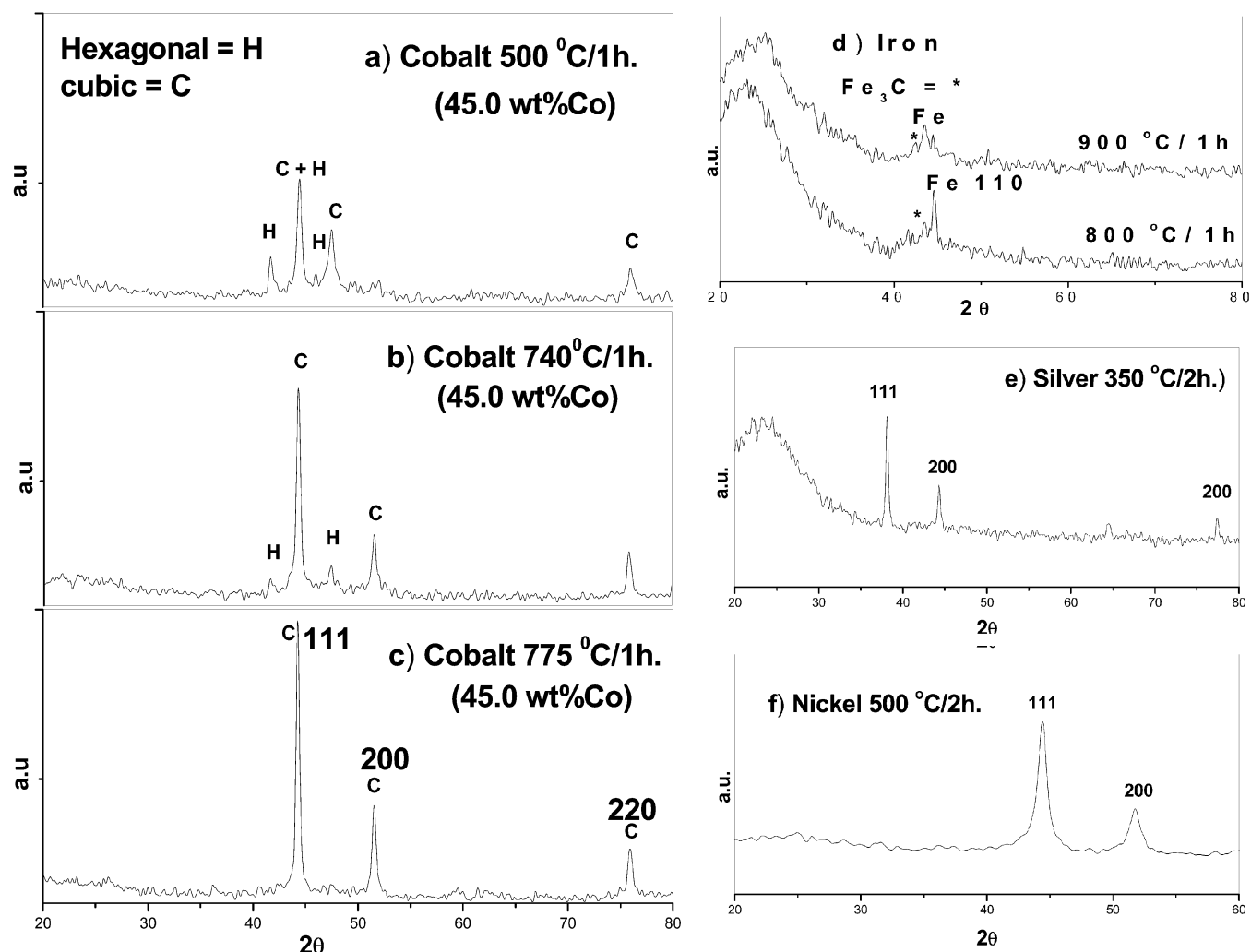

Figure 5. XRD patterns of powders containing transition metals: (a) SiO₂:Co (45.0 wt % Co), annealed 500 °C/1 h, in N₂; (b) SiO₂:Co (45.0 wt % Co), annealed 740 °C/1 h, in N₂; (c) SiO₂:Co (45.0 wt % Co), annealed 775 °C/1 h, in N₂; (d) SiO₂:Fe (10.0 wt % Fe), annealed 900 °C/1 h and 850 °C/1 h, in N₂; (e) SiO₂:Ag (1.0 wt % Ag), annealed 350 °C/2 h in air; (f) SiO₂:Ni (23.0 wt % Ni), annealed 500 °C/2 h, in N₂.
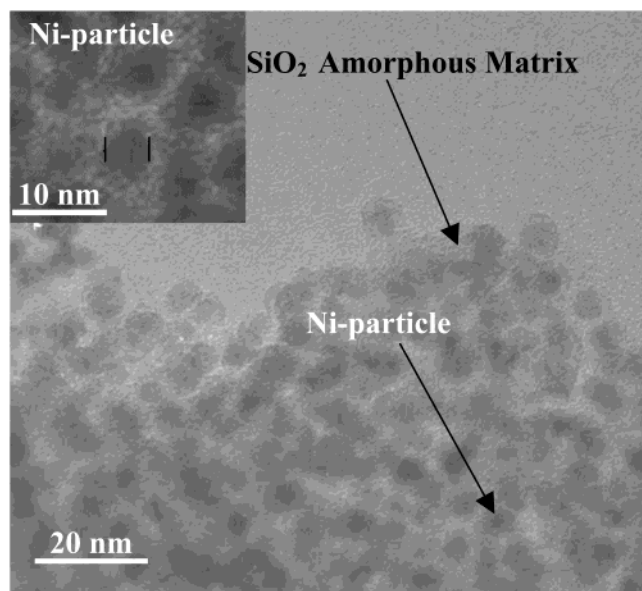
Figure 6. (a) BF-TEM image of the nanocomposite with SiO₂:Ni (23.0 wt % Ni). Sample heat-treated for 2 h at 500 °C, in a N₂ atmosphere.

detected. A similar result was reported by Tsang et al.[15,16] The increase of the heat-treatment temperature led to the increase of iron carbide phase content, which suggests there was a reaction between the iron nanoparticles and the amorphous carbon.

The SiO₂:Ag ($\approx$1.0 wt %Ag) nanocomposite system showed the lowest temperature for the metallic phase formation. Metallic silver was detected after a heat treatment at 350 °C, for 2 h. We observed that the Ag metallic phase was formed even in the presence of an oxidizing atmosphere such as air (see Figure 5e).

3.3. Microstructure Characterization. Figure 6 shows a bright-field (BF) TEM image of the SiO₂:Ni sample with high Ni concentration ($\approx$23.0 wt %Ni). We can observe Ni nanoparticles (dark spots in the photograph) well dispersed in an amorphous SiO₂ matrix. BF-TEM analysis revealed that the Ni particles present a homogeneous particle size distribution, with a mean particle size of 4.7 nm.

Figure 7 shows BF-TEM images of the SiO₂:Co nanocomposite ($\approx$45.0 wt % Co) annealed at different temperatures. The SiO₂:Co system also presents nanometric metallic particles dispersed in an amorphous phase. A HRTEM analysis of the SiO₂:Co nanocomposite annealed at 740 °C (Figure 7b) presents Co particles encapsulated by an ordered carbon layer. It is interesting to point out that ordered carbon is only observed near the Co nanoparticles. The spacing between carbon layers is approximately 0.337 nm. This interlayer spacing, which is close to the one of graphite d_{002} planes (d_{002} = 0.338 nm), is characteristic of the turbostatic graph-

(14) SiO₂ (quartz) was used as an external standard to correct the diffraction peak broadening due to the experimental X-ray setup.
(15) Tsang, S. C.; Chen, Y. K.; Harris, P. J. F.; Green, M. L. H. *Nature* **1994**, *372*, 159.
(16) Tsang, S. C.; Qu, J.; Harris, P. J. F.; Fu, Q. J.; Zhang, N. *Chem. Phys. Lett.* **2000**, *322*, 553.
(17) Babonneau, D.; Cabioc׳h, T.; Naudon, A.; Girad, J. C.; Denanot, M. F. *Surf. Sci.* **1998**, *409*, 3358.
(18) Dresselhaus, M. S.; Dresselhaus, G.; Sugihara, K.; Spain, I. L.; Goldberg, H. A. In *Graphite Fibers and Filaments*; Springer-Verlag: Berlin, 1988; p 42.
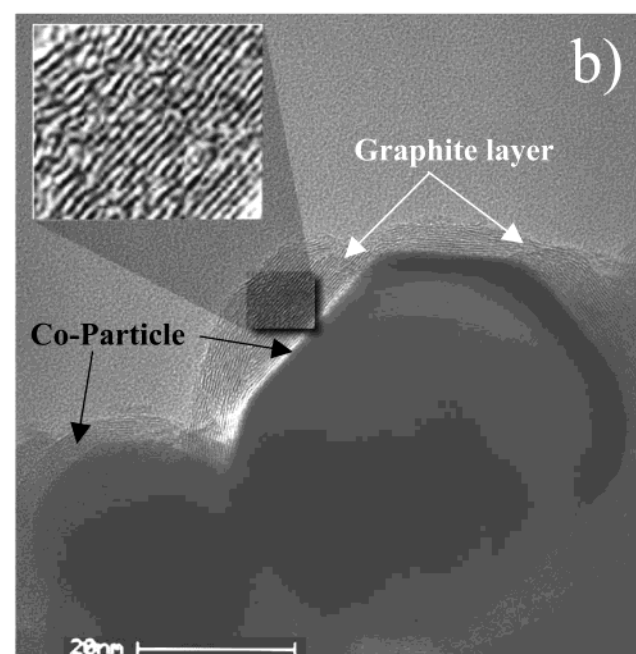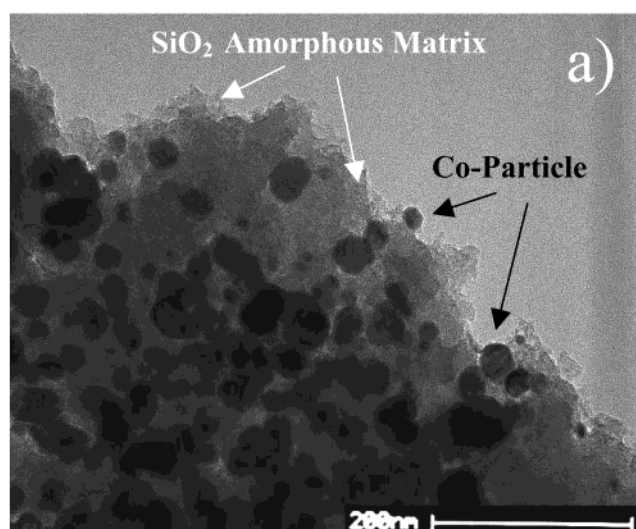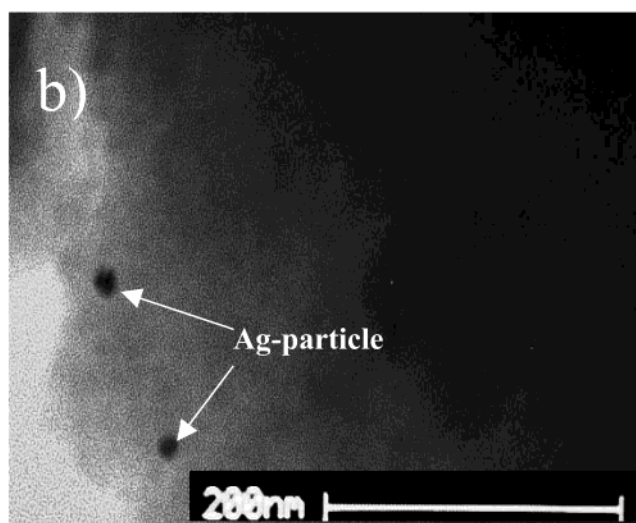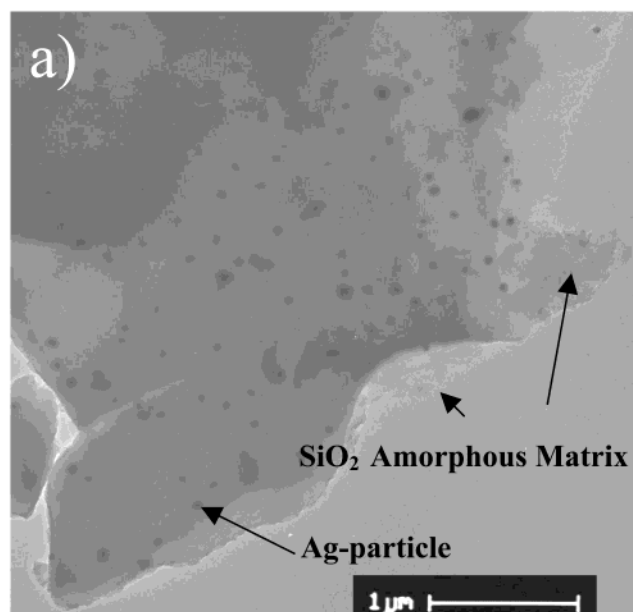

Figure 7. BF-TEM images of the nanocomposites with SiO₂:Co (45.0 wt % Co). (a) Sample heat-treated for 1 h at 500 °C in a N₂ atmosphere; (b) annealed for 1 h at 740 °C, in a N₂ atmosphere.

ite.[17,18] Furthermore, the graphite layers seem to be stacked parallel to the surface of the particles, suggesting a catalytic effect of the metal, to obtain ordered carbons. The presence of the residual carbon can play an important role in the mean particle size and the surface oxidation of the cobalt nanoparticles.

The microstructure characterization of the SiO₂:Ag nanocamposite, annealed at 500 °C for 1 h under a N₂ atmosphere, reveals a uniform distribution of the Ag particles in an amorphous matrix (Figure 8a). The BF-TEM image of Figure 8b presents Ag particles with the size in the range of 10−20 nm. This sample was obtained after pyrolysis in air.

TEM micrographs of the SiO₂:Fe nanocomposite (Figure 9a−c), annealed at 900 °C for 1 h, showed that it contains iron nanoparticles of very uniform size (10−20 nm). All the particles were embedded in a highly disordered material (silica and carbon). The SiO₂:Fe

Figure 8. BF-TEM images of the nanocomposites with SiO₂: Ag (1.0 wt %Ag). (a) Sample heat-treated for 1 h at 500 °C, in a N₂ atmosphere; (b) annealed for 1 h at 350 °C, in an air atmosphere.

Figure 9. BF-TEM images of the nanocomposites with SiO₂: Fe (10.0 wt % Fe). (a) and (b) sample heat treatment for 2 h at 900 °C, in a N₂ atmosphere; (c) annealed for 1 h at 800 °C in a N₂ atmosphere.

samples also show regions with ordered and amorphous carbon layers around iron particles, as illustrated in Figure 9c. The phenomenon of catalytic graphitization over metallic particles is well-known,[16] but the mechanism through which graphitization is promoted by the presence of a second phase is not well understood. In some cases, it is believed that the carbon is dissolved in the metal or metal carbide and reprecipitated as graphite. In other cases the metal or metal carbide particles may simply act as templates for the epitaxial growth of graphite.[15]

The images of the TEM analysis indicate that the Ni, Co, Ag, and Fe nanoparticles are embedded within the SiO₂ matrix and not deposited on the surface. The mean particle size values estimated by TEM are in good agreement with the crystallite sizes characterized by XRD (see Table 1).

The formation of ordered carbon was more easily observed for the case of cobalt, due to the higher heat-treatment temperature. The different morphologies and
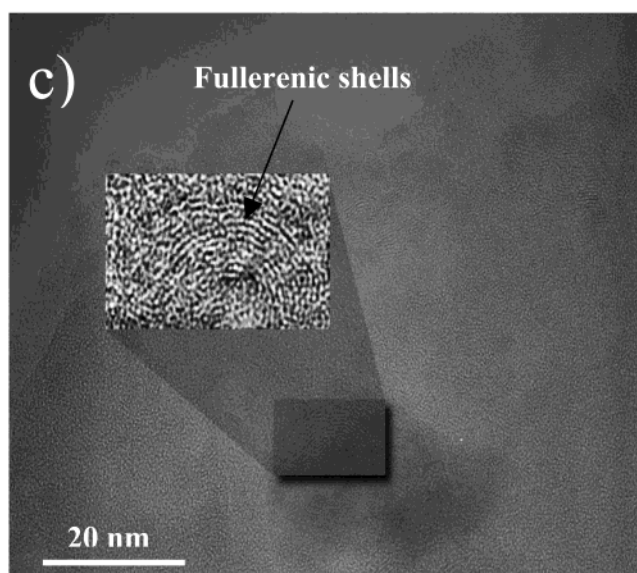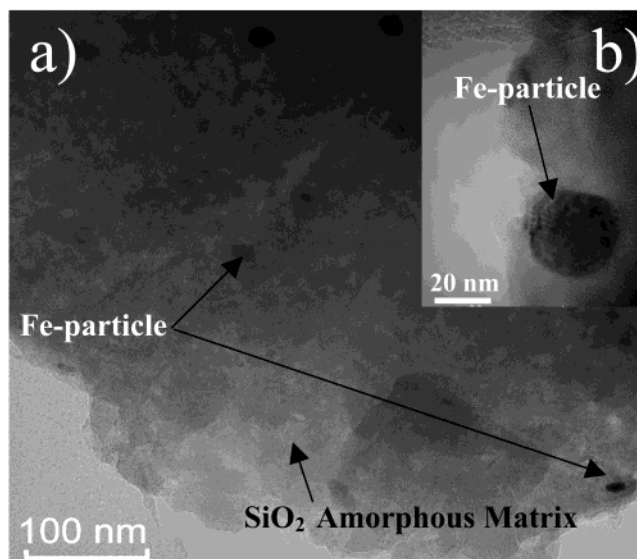
different concentrations of ordered carbon formed for all the metallic systems studied are now starting to be investigated and will be later reported.

3.4. General Discussion. The results herein presented showed that, during the polymeric precursor synthesis, a hybrid polymer based on a polyester, with Si and C present in the macromolecule chain, is formed. The transition metal cation can be chelated by a free carboxyl group or even be arrested within the macromolecule. In both cases, the cation will be well distributed throughout the polymeric precursor, which ensures a good dispersion of the metallic nanoparticles after the pyrolysis step.

During the pyrolysis step occurs the macromolecule breakage, which will result in an amorphous matrix formed basically by SiO₂ and carbon. The CO/CO₂-rich atmosphere during the pyrolysis will promote the reduction of the metallic salt, resulting in metallic nanoparticles. The reduction temperature is associated

with the metal reducibility in CO. These particles are preferentially embedded within the amorphous matrix and not deposited on the matrix surface. The formation of ordered carbon around the metal nanoparticles was also observed. These microstructural features, that is, the metal nanoparticles embedded in the amorphous matrix and the carbon layer, can result in a low nanoparticle growth rate at elevated temperatures and low surface nanoparticle oxidation. The method herein presented can be used to process nanostructured material for catalytic applications or even with interesting magnetic properties.

4. Conclusion

The experimental results herein presented allowed us to conclude the following:

(a) The ^{13}C NMR and FT-Raman spectroscopic results showed the formation of the Si–CA complex formation, with the preferential reaction of Si with the terminal –COOH group of CA and the formation of a polymeric hybrid precursor.

(b) During the pyrolysis occurs the simultaneous formation of an amorphous matrix and metal nanoparticles, with particle sizes in the range of 3–40 nm. The temperature of metal formation depends on the nature of the metal and its reducibility in the CO generated during the pyrolysis.

(c) The SiO_2:Co and SiO_2:Fe systems showed the formation of ordered carbons on the nanoparticles surface.

(d) The method herein presented is suitable to process several transition SiO_2:metal nanocomposites, with the metal nanoparticles embedded in the amorphous matrix.